9-9-2020

High Layer Uniformity of 2-d Materials Surprisingly From Broad Features in Surface Electron Diffraction

Shen Chen
Iowa State University and Ames Laboratory, schenad@iastate.edu

Michael Horn von Hoegen
Iowa State University

Patricia A. Thiel
Iowa State University

Adam Kaminski
Iowa State University and Ames Laboratory, adamkam@ameslab.gov

Benjamin Schrunk
Iowa State University and Ames Laboratory, bschrunk@ameslab.gov

See next page for additional authors

High Layer Uniformity of 2-d Materials Surprisingly From Broad Features in Surface Electron Diffraction

Abstract

Paradoxically a very broad diffraction background, named the Bell-Shaped-Component (BSC), has been established as a feature of graphene growth. Although the BSC has been present in the earlier literature it has been ignored. Recent diffraction studies as a function of electron energy have shown that the BSC is not related to scattering interference. The BSC is a very strong effect, but its origin is still unclear. Here, additional experiments are carried out as a function of temperature while monitoring changes in the intensity of different spots over the range that single-layer-graphene (SLG) grows. Quantitative fitting of the profiles shows that the BSC follows the increase of the G(10) spot, proving directly that BSC is an indicator of high quality graphene. Additional metal deposition experiments provide more information about the BSC. The BSC is insensitive to metal deposition and it increases with metal intercalation, because a more uniform interface forms between graphene and SiC. These experiments support the conclusion that the BSC originates from electron spatial confinement within SLG and surprisingly it is an excellent measure of graphene uniformity, instead of film disorder.

Disciplines

Biological and Chemical Physics | Materials Chemistry | Materials Science and Engineering | Physical Chemistry

Comments

This document is the unedited Author's version of a Submitted Work that was subsequently accepted for publication in *The Journal of Physical Chemistry Letters*, copyright © American Chemical Society after peer review. To access the final edited and published work see DOI: 10.1021/acs.jpclett.0c02113. Posted with permission.

Authors

Shen Chen, Michael Horn von Hoegen, Patricia A. Thiel, Adam Kaminski, Benjamin Schrunk, Thanassis Speliotis, Edward Henry Conrad, and Michael C. Tringides

High layer Uniformity of 2-d Materials surprisingly from Broad Features in Surface Electron Diffraction

S. Chen[1,2] M. Horn von Hoegen[4], P. A.Thiel[1,3] A. Kaminski[1,2], B. Schrunk[1,2]
T. Speliotis[5], E.H.Conrad[6] and M.C.Tringides[**.1,2]

[1]Ames Laboratory - U.S. Department of Energy, [2]Department of Physics and Astronomy,

[3]Department of Chemistry Iowa State University, Ames, IA 50011, U.S.A

[4]Department of Physics and Center for Nanointegration CENIDE, University of Duisburg-Essen, Lotharstrasse 1, 47057 Duisburg, Germany

[5]Institute of Nanoscience and Nanotechnology, National Center for Scientific Research Demokritos, Agia Paraskevi, 15310, Athens, Greece

[6]Department of Physics Georgia Technology Institute 837 State Street Atlanta, Georgia 30332-0430

ABSTRACT

Paradoxically a very broad diffraction background, named the Bell-Shaped-Component (BSC), has been established as a feature of graphene growth. Recent diffraction studies as a function of electron energy have shown that the BSC is not related to scattering interference. Here, additional experiments are carried out as a function of temperature over the range that single-layer-graphene (SLG) grows. Quantitative fitting of the profiles shows that the BSC follows the increase of the Gr(10) spot, proving directly that the BSC indicates high quality graphene. Additional metal deposition experiments provide more information about the BSC. The BSC is insensitive to metal deposition and it increases with metal intercalation, because a more uniform interface forms between graphene and SiC. These experiments support the conclusion that the BSC originates from electron confinement within SLG and surprisingly it is an excellent measure of graphene uniformity.

Corresponding author: mctringi@iastate.edu 1515 294 6439

Graphene has been studied extensively with several complementary techniques to relate its structural quality to its electronic properties and band structure[1-4]. Clear understanding of most structural issues has been attained (i.e., atom position, thickness, stacking, relative layer orientation, band structure variation with graphene thickness, etc.) with both real space and reciprocal space techniques. One important persisting requirement is to grow large domains of single thickness, so the unique properties of a homogeneous, spatially extended 2-d material are fully realized. With the more recent emphasis on other 2-d materials beyond-graphene (with similar bonding and electronic properties), the same requirements of uniform thickness and large domain size are presenting a similar and more challenging problem[5]. For epi-graphene grown on SiC this is especially important because growth is carried out at high temperatures (above~1200° C); where Si evaporates from several SiC bilayers while the remaining C diffuses and forms a uniform graphene layer. However within a narrow range (~200° C) the grown thickness changes from buffer layer (BL) to single-, bilayer-, and multi-layer graphene. Because the temperatures where a given thickness is grown are high and different regions grow at different rates, the growth process most likely results in some mixture of layers. Since graphene properties change with thickness it is essential to measure the areas covered by each layer. When metal intercalation is used to alter graphene's properties, layer distribution is important because boundaries between layers of different thickness are likely entry portals for the intercalated atoms.

Recently it was shown with surface electron diffraction[6] that a surprisingly very broad component develops around the (00) and Gr(10) spots for both graphene on SiC and for graphene on metals. This bell-shaped-component (BSC) has a width ~50% of the graphene Brillouin zone (BZ). This unusually broad and intense component does not indicate a rough and disordered film as expected from textbook diffraction[7], but instead shows a well ordered single layer film. The BSC paradoxically has been present in the earlier graphitization experiments of SiC, but it has never been mentioned.[8-13] In these earlier studies several pioneering characterization experiments were performed confirming the unusual properties of graphene, which indicates that the BSC is important. It also demonsrates that the origin of the BSC must be general and fundamental. Since these results are very unintuitive and film uniformity is so important for all 2-d materials, in this work we provide additional information confirming that the BSC is a measure of high graphene quality. Spot profile experiments were analyzed as a function of energy, to show that the measured parameters for the broad and narrow diffraction components, do not follow the variation of the profile shape expected from scattering interference[7]. Annealing experiments to record the evolution from BL to SLG show quantitatively that the BSCs, both around the (00) and Gr(10) spots, follow closely the growth of the Gr(10) spot. This confirms directly that the BSC is intrinsically related to graphene quality. Metal deposition experiments further support the unusual character of the BSC. These experiments show that the intensity at the BSC center does not decrease, as would be expected from destructive interference between diffracted waves from deposited metal and substrate atoms. Intercalation experiments that decouple graphene from SiC show stronger BSC, which also suggests the BSC is related to electron spatial confinement within a single layer. These experiments add additional support to the hypothesis that the BSC originates from the high precision of locating an electron's position normal to the graphene sheet[14]. The high electron confinement normal to the surface generates a large spread in the graphene electron's wavevector. The wave vector spreading is transferred to the diffracted electrons via the interaction between graphene electrons and incident beam electrons. By monitoring the evolution of the BSC with temperature, we can determine the exact conditions for uniform thickness graphene to form.

The technique can also be used to clarify the growth conditions for the recently discovered semiconducting phases of the BL[15,16].

The substrates used in the current experiments were 4H-SiC(0001) purchased from Cree, Inc. The samples were graphitized in UHV (P~1×10^{-10} torr) by direct current heating repeatedly to ~1200°-1400° C for tens of seconds. The layer thickness (whether single layer or bilayer) was controlled by the heating rate: faster rates (400° C/s) result in single layer graphene (SLG) while slower rates (~40° C/s) result in bilayer graphene[17-21].

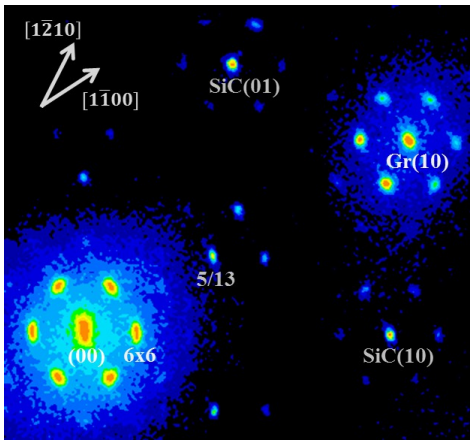

Fig. 1 Diffraction pattern at 194 eV of clean graphene which is a mixture of BL and SLG. The 5/13 spot and the two adjacent 6x6 spots indicate that a fraction of the surface is BL and the Gr(10) spot indicates that the rest is SLG. BSC is seen around the (00) and the Gr(10) but not the SiC(10) spots.

Fig. 1 shows the 2-d electron diffraction pattern over one fourth of the BZ (at an electron energy of 194 eV) for clean graphene that was grown at 1240° C. The presence of a strong 5/13 spot and the two adjacent quasi 6x6 spots indicate that part of the surface is BL[10]. The strong Gr(10) spot indicates that the rest is SLG. Although the 6x6 spots which originate from the graphene-SiC interface are actually incommensurate, they are commonly called "buffer layer spots" in the video LEED literature. In addition to the 6x6 spots surrounding all fundamental spots, the 5/13 spot is the strongest LEED spot among the spots from the quasi-(13x13) BL-SiC incommensurate supercell. It is the most sensitive to the presence of BL. No BSC is ever seen around SiC(10), confirming that the origin of BSC is related to graphene electrons. When heated to 1300° C the 5/13 spot decreases and the Gr(10) spot becomes stronger signaling the formation of complete SLG, as seen in previous studies[4, 8-13].

These measurements have the advantage that the BSC can be separated from the narrow component of the (00) and the Gr(10)[6]. A diffraction profile decomposes into two component: a narrow component which in typical surface diffraction measures the long range order in the system and the total number of scatterers; and a broad component reflects short range order and domain size. The 00 energy dependent profile analysis, for the film grown at 1300° C, is summarized in Fig. 2. In Fig. 2(a) the integrated area of the narrow component is shown in black and the FWHM of the narrow component in pink. Maxima in the peak area are observed at 144 eV and 104 eV and minima at 124 eV and 160 eV. No oscillations are observed for the FWHM, confirming graphene's

homogeneity. The lack of FWHM oscillations shows that the domain size exceeds the coherence length of SPA LEED. In Fig. 2(b) the integrated area of the BSC of the (00) is shown in black and the FWHM of the BSC is shown in blue as a function of electron energy. Maxima are observed at 144 eV and 104 eV and minima at 124 eV and 160 eV, the same energies as for the narrow component, thus ruling out that BSC is a result of scattering interference between adjacent domains[7]. The overall increase with energy confirms the confinement mechanism as the origin of the BSC, since for a larger Ewald sphere the increase in $\Delta k_{\parallel}$ for the same Δk_z (and therefore the FWHM of the BSC) is larger. The size of the symbols corresponds to the error bars. From the same graph it is seen that the FWHM oscillates with $\Delta S \approx 1$ which corresponds to single graphene step height. In typical surface diffraction the FWHM and integrated areas of the broad component are correlated,[7] because the increase of the broad component is caused by transferring intensity from the center of the profile to lager wavevectors at the "wings". Instead, for graphene the FWHM and integrated area of the BSC component as seen in Fig.2 (b) they are anti-corelated which independently confirms the unusual origin of the BSC.

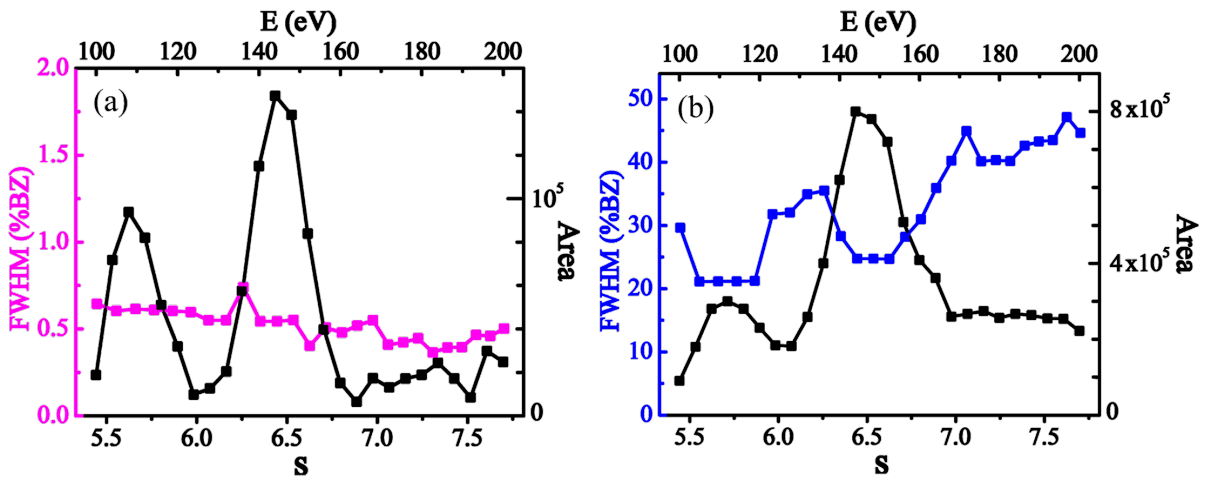

Fig. 2 The SLG profile analysis of the (00) spot for a film grown at 1300° C. (a) The integrated area of the narrow component is shown in black and the FWHM of the narrow component in pink as a function of energy (top scale) or the normalized phase $s=d_g(\Delta k_z)/2\pi$ with $d_g=0.33$ nm and Δk_z the normal momentum transfer (bottom scale). No oscillations are observed for the FWHM indicating that the graphene domain size exceeds the coherence length of SPA LEED. This confirms the graphene's homogeneity. (b) The integrated area of the BSC of the (00) is shown in black and the FWHM of the BSC is shown in blue as a function of electron energy. Maxima are observed at the same energies as for the narrow component.

Because of SPA-LEED's higher resolution and because the spots are studied quantitatively, annealing experiments were carried out to follow the growth of graphene from BL to SLG as a function of temperature. Since the narrow components of both spots measure the grown SLG and are sensitive to layer uniformity, it is possible to test how the BSC (as it changes with temperature) relates to the grown graphene quality. Four profiles are shown along $[1\bar{1}00]$ in fig.3 obtained after heating for 15 s few (5-6) times at each temperature 1200° C, 1240° C, 1280° C and 1300° C. The

four profiles in fig.3 are shown bottom to top from low to high temperature. They are shifted for clarity with the bars on the ordinate axis marking the same intensity. The Gr(10) and (00) increase while the 5/13 decreases in intensity, as the SLG progressively covers the BL. The spot evolution can be analyzed quantitatively by fitting the profiles with Lorentzian functions described by a 3/2 exponent at the denominator (LRZ-3/2). This is a better choice than Lorentzian function (the exponent is -1) both for the narrow and BSC components. For the narrow component the LRZ-3/2 function corresponds to a much sharper domain size distribution of the grown graphene. For the BSC component it reflects the sharper distribution expected for the momentum transfer of the graphene electrons, that is causing the BSC based on the confinement mechanism. However the origin of the BSC is not related to the surface morphology and as noted before it is correlated to the narrow component. This major result is independent of the choice of the fitting function whether LRZ-3/2 or LRZ, because it involves only the integrated areas of the narrow and BSC components.

Two components were used for the (00) and Gr(10) spots, the narrow and the BSC. From the fits, the areas of the narrow (00), the BSC of (00), the narrow of Gr(10), the BSC of Gr(10), the 5/13 and the 6x6 spots (along $[1\bar{2}10]$) were extracted. The areas were normalized to the integrated area over the measured BZ (for each profile along the two directions) to remove effects due to differences in beam current or scattering factors. After the normalization, all the integrated areas have a monotonic dependence on temperature as seen in table I. The integrated area of the BSC around the (00) and the integrated area of the BSC around Gr(10) follow the integrated area of the narrow component of the Gr(10). As the area of Gr(10) increases by a factor of 10 the areas of the two BSCs increase by a factor of 4. The schematic to the right side of fig. 3 shows the changing surface morphology, corresponding to each of the profiles on the left. It shows graphically the growth of SLG, as it finally fully covers the BL.

The experiments discussed so far show that the BSC is a diagnostic of high quality graphene, The question that remains is how it is generated? A likely origin is related to the thickness uniformity of graphene, of a single layer $\Delta z=d_g=0.33nm$[13], that extends without interruption over steps. It provides perfect confinement of the graphene electrons normal to the surface. From the uncertainty principle $\Delta p_z.\Delta z \geq \hbar$ we have that $\Delta\kappa_z \approx 1/d_g$ is the spread of κ_z (the normal component of the electron wavevector of the graphene electrons). This range was measured directly with ARPES[14] and it was maximal for SLG, (decreasing with m=2,3 as the graphene thickness md_g

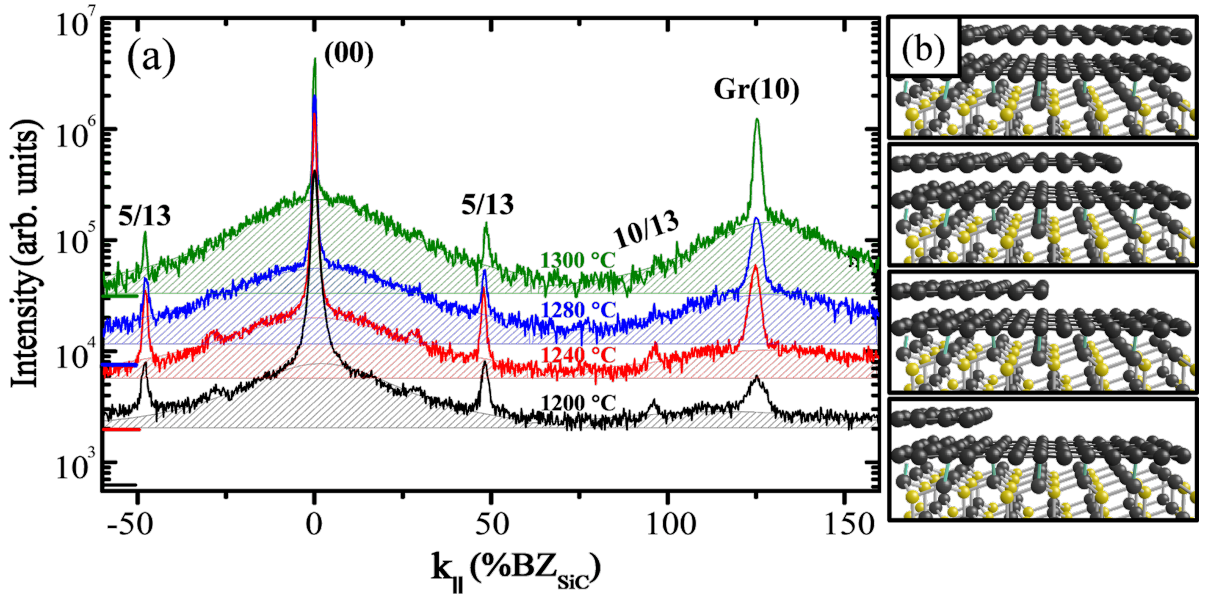

Fig.3 (a)The growth of graphene from BL to SLG followed as a function of temperature. Four profiles are shown along $[1\bar{1}00]$ obtained after heating few times for 15 s at 1200° C, 1240° C, 1280° C and 1300° C respectively. They are shifted for clarity with the bars on the ordinate axis marking the same intensity. The evolution of these profiles can be analyzed quantitatively by fitting them with LRZ-3/2 functions. From the fits the areas of all spots (narrow (00), BSC of (00), narrow Gr(10), BSC of Gr(10), the 5/13 and the 6x6 spots along $[1\bar{2}10]$) were calculated. The areas were normalized to the total integrated area (shown by the shaded areas) over the measured BZ. After the normalization the Gr(10) and (00) increase monotonically with temperature, while the 5/13 decreases in intensity. (b) Schematics of the surface morphology corresponding to the measured diffraction profiles to the left.

increases). The uncertainty $\Delta\kappa_z$ generates an uncertainty in the z component Δk_z of the momentum transfer to the diffracted electrons via graphene-electron with beam-electron interaction. Because scattering is elastic with electron energy E=constant, a spread Δk_z in the diffracted electrons generates a spread in their parallel momentum transfer $k_{||}$. The momentum transfer (Δk_z, $k_{||}$) of the diffracted electrons is constrained to move along the Ewald sphere by energy conservation; with each value of k_z within Δk_z corresponding to a different value of $k_{||}$, thus generating the BSC.

Additional evidence supporting this mechanism is seen in μ-LEED when there are layers of different thickness in the field of view. The thickness can be identified from I-V reflectivity curves. μ-LEED experiments were performed on G/SiC samples with regions of thickness m= 1-, 2-, 3-, 4- layers[22]. Micro-diffraction patterns were recorded from areas of a single thickness. The Gr(10) becomes stronger and the $6\sqrt{3}$ spots weaker with increasing m. A BSC is present around the Gr(10) and its width decreases with m as expected from the decreasing spread of the electron momentum within thicker layers $\Delta\kappa_z \approx 1/md_g$.

Table I . Integrated areas of the narrow component of the Gr(10), of the BSC around the (00) spot, and of the BSC around the Gr(10) spot[a].

temperature [°C]	Gr(10) narrow	(00) BSC	Gr(10) BSC
1200	0.016	0.292	0.091
1230	0.063	0.371	0.143
1280	0.093	0.596	0.303
1300	0.180	0.760	0.379

[a] The two BSCs integrated areas follow the area of the narrow component of the Gr(10) with annealing temperature. Since the narrow Gr(10) component is a measure of SLG, this shows that the two BSCs also reflect high quality graphene.

The increase of the FWHM with electron energy already discussed for fig.2 is consistent with the confinement scenario: at higher energies the radius of the Ewald sphere is larger, so the same spread in $\Delta\kappa_z$ causes larger change in the parallel component $k_{||}$ and therefore larger FWHM of the BSC. The BSC is also seen in truly free standing graphene which was used for ultrafast LEED experiments[23]. The recorded diffraction pattern shows a strong BSC which extends to a large fraction of BZ (~40%) (even for beam energies ~450 eV), similar to the BSC seen by regular LEED.

The unusual behavior of the BSC can also be observed in adsorption experiments, if a second element is either deposited on top of or intercalated below graphene. Scattering between the deposited and substrate atoms should decrease the diffracted intensity at the profile center: because of different scattering phase (the deposited and substrate atoms are at different heights) and/or scattering factor (difference in the atomic structure of the deposited and substrate atoms).

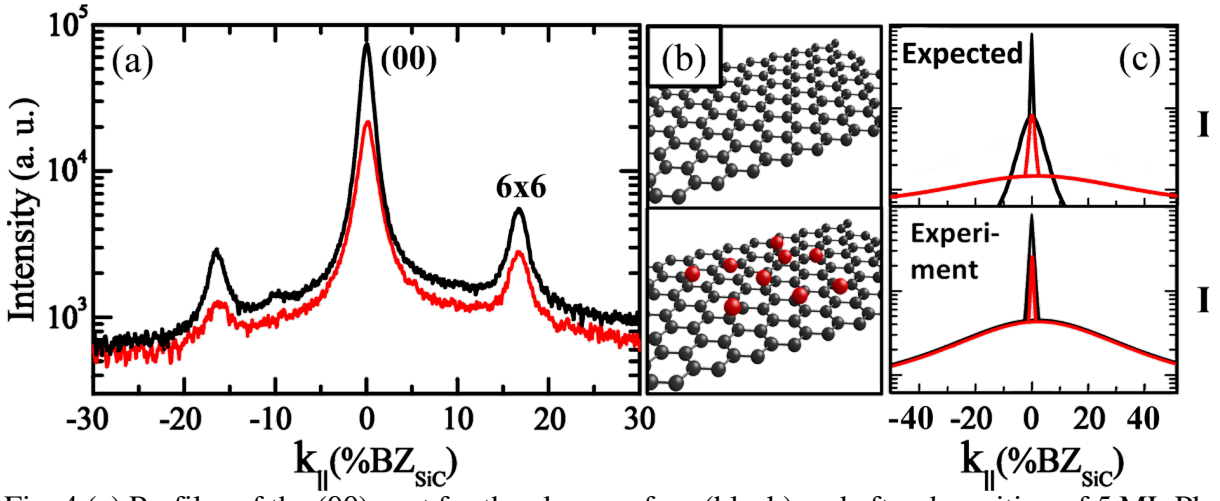

Fig. 4 (a) Profiles of the (00) spot for the clean surface (black) and after deposition of 5 ML Pb at -180° C (red). The same color scheme is used for the schematics in (c). The narrow component intensity drops by a factor of 3 (as well as the 6x6 intensity) expected from destructive interference, between the Pb islands and bare areas. However the BSC intensity drops by less than 10% and its FWHM is practically unchanged. (b) Schematic in the middle shows the clean surface (black) and the surface after a small deposition of Pb (red balls). (c) Schematic (top) expected pattern if generated by scattering interference, both the narrow and broad components should drop in intensity; (bottom) schematic of the experimental results showing that the narrow component drops but the BSC does not drop in intensity and does not broaden.

Fig. 4(a) shows how the diffraction intensity behaves after deposition of 5ML Pb at -180° C. The Pb is very mobile and is known to form multilayer islands that cover 40% of the surface[24]. As can be seen from fig.4 (i.e., from the difference in the logarithmic intensity scale between black and red profiles at $k_{||}=0$), the narrow diffraction component drops by a factor of 3 (as well as the 6x6 intensity) expected from scattering interference. (The color scheme in fig. 4 shows the clean surface (black) and after Pb deposition (red)). However the BSC intensity and shape are practically unchanged; its FWHM increases only by 5%, while its peak intensity drops by less than 10%. The schematic fig.4(b) shows the clean and adsorbed surfaces; fig.4(c) shows schematically what is expected from scattering interference (top) and what is observed experimentally (bottom). For scattering interference both components drop in intensity at $k_{||}=0$ as intensity shifts to larger wavevectors, while total intensity conserved. Experimentally only the narrow component drops and the BSC is practically unchanged, showing that the BSC does not originate from destructive intereference, between deposited and substrate atoms. A larger change in shape and area of the BSC should be expected for the much rougher morphology (i.e., beating of the 3-d Pb islands with the flat substrate) after deposition. This result after metal adsorption is also seen in fig. 8 of our previous publication[25]. After 0.12 ML Dy is deposited the narrow component drops ~50%, while the BSC remains constant.

Concerning the BSC similar diffraction intensity loss at the profile center is expected from scattering interference, if the metal is intercalated below graphene, because the film uniformity will be interrupted. Metal intercalation is mostly a kinetic process, i.e., how metals deposited on top move below graphene. Besides finding the temperature for a given metal to intercalate, it is also important to know the location and the amount of the intercalated metal, since depending on the metal location, (whether between SLG and BL or between BL and SiC), graphene will have different properties.

We focus on how the BSC changes with intercalation using Dy as a case study. We deposit 2 ML of Dy at RT on SLG; then progressively anneal to higher temperature. Starting from 850° C the intensity of all spots (00, Gr (10), 6x6 etc.) starts to drop indicating that Dy intercalates and occupies locations on top and between different graphene layers below. By heating to higher constant temperature, for different annealing times, the most stable binding location can be identified, since all intercalated atoms diffuse and bond to this location.

As discussed next, such experiment reveals again that the BSC is not sensitive to scattering interference and confirms the confinement mechanism. After the 2 ML of Dy are annealed by short 15 s flashes at ~1200° C, profiles are shown after the first flash (pink) and after 13 flashes (blue) in fig.5 with the electron energy 192 eV. Profiles in fig.5(a) are along the $[1\bar{2}10]$ direction. They show that the SiC(10) spot and the 6x6 spots surrounding it decrease in intensity which indicates intercalation between BL and SiC, because these spots originate from the BL-SiC interface.. The two schematics at the top of fig. 5 show the change in the Dy adatom distribution. After the first flash they are more randomly distributed among all locations between the top layers, but as shown in the right schematic, at the end they are uniformly bonded only between BL and SiC. This causes the intensity decrease of the 6x6 and SiC(10) spots until eventually they disappear. Profiles in fig.5(b) are along *t*he $[1\bar{1}00]$ direction. The (00), Gr(10), the BSC around (00) and the BSC around Gr(10) spots grow in intensity as the Dy atoms are transferred to more ordered layer between the BL and SiC. Both the area of the BSC around Gr(10) and around (00) grow and the corresponding FWHMs decrease by ~15% after the last flash.

The insertion of the Dy atoms at the SiC-BL interface and the conversion of the SLG to bilayer graphene, provide more uniform interface for the graphene electrons, when compared to the result of the first flash, with the Dy atoms randomly distributed in all the layers above SiC. The two schematics at the top of fig. 5 show the change in the Dy adatom distribution. After the first flash they are more randomly distributed among the locations between the top layers, but as shown in the right schematic, at the end they are uniformly bonded only between BL and SiC. The increase of BSC is primarily because the distribution of the intercalated atoms below graphene becomes less random, as they diffuse and bond only at the BL-SiC interface. After intercalation the BL decouples electronically from SiC, which effectively results in better condition for the electron localization within a layer of uniform thickness. This can be a secondary reason for the increase of BSC. The decrease of the FWHM is also a result of the conversion of the BL to graphene and the change of the SLG to bilayer graphene. This decreases the wavevector spread $\Delta\kappa_z$ due to electron confinement and therefore it decreases the FWHM of the BSC. The increase of BSC

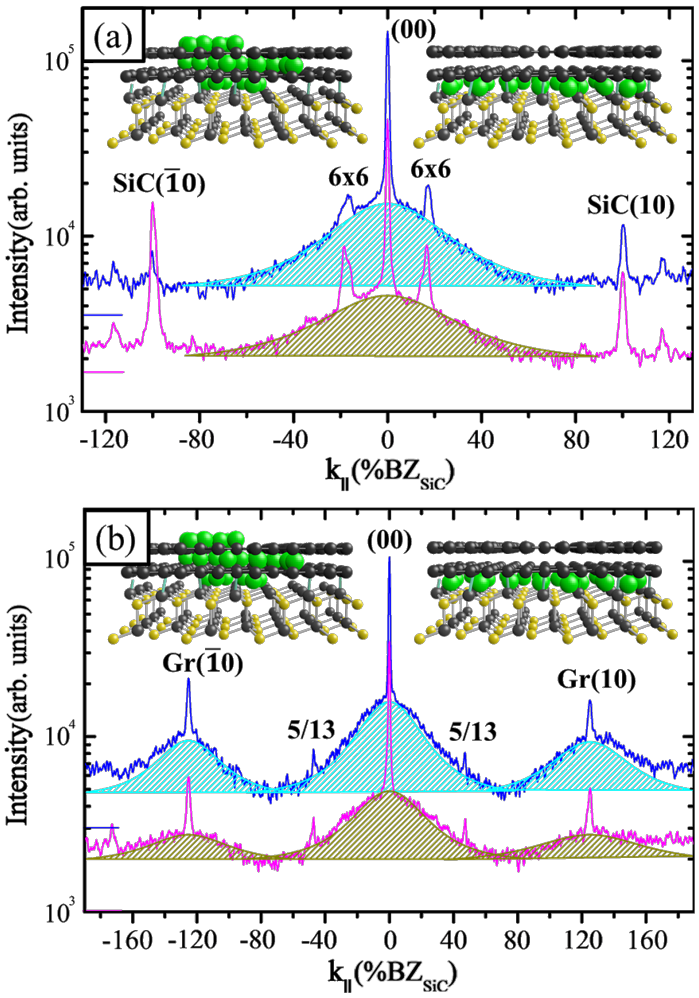

Fig. 5 (a) Profiles of SLG after 2 ML Dy deposited at RT followed by a number of flashes, each flash for 15 s at 1200° C; after 1 flash (pink) and after 13 flashes (blue), electron energy 192 eV.(a) Profiles along $[1\bar{2}10]$). The SiC(10) spot and the 6x6 spots surrounding it decrease in intensity which indicates intercalation between BL and SiC.(b) Profiles of SLG along $[1\bar{1}00]$. The (00), Gr(10), the BSC around (00) and the BSC around Gr(10) spots grow in intensity as the Dy is transferred between the BL and SiC. The left schematic shows the surface after the initial flash with Dy bonded randomly between layers. The right schematic shows the surface after the last flash with all Dy as a more uniform intercalated layer. The BSC grows in intensity and its FWHM decreases after the last flash.

intensity is also seen in hydrogen intercalation experiments cf. fig.4 by T. Langer et al.[26] which shows stronger BSC for the intercalated than pristine film. The experiments described in the current work show the unusual behavior of the BSC under a wide range of conditions; they do not originate from destructive interference when metal atoms are adsorbed on or below a substrate.

Characterization of our samples with strong BSC using other techniques (STM, ARPES), its extensive presence in numerous literature experiments and in experiments for graphene grown on metals is described in Supplementary Materials[27].

Unusual broad profiles were observed with FWHM as large as 35%BZ (similar to the current studies) with LEEM and μ-LEED experiments in suspended and supported (on SiO_2) graphene flakes[28]. They have been attributed to graphene roughness. However the trends of the variation of the FWHM with control parameters are similar to the variation of the FWHM of the BSC already discussed: the FWHM increases with energy, decreases with graphene thickness and decreases with increasing disorder.

In conclusion an unusually broad diffraction feature, the BSC has been strangely observed in numerous electron diffraction studies, totally unexpected because graphene is a highly uniform film. The energy dependence of spot profiles shows that the BSC cannot be related to scattering interference from adjacent terraces, as common in all other films. Annealing experiments monitoring the growth of SLG have shown that the BSC integrated area is highly correlated to the growth of Gr(10), thus suggesting that the BSC is also a reliable diagnostic of graphene quality. Metal deposition and intercalation experiments show that the BSC grows stronger and with a reduced FWHM after complete metal intercalation, a result of stronger confining condition of the graphene electrons and decoupling of graphene from the substrate. Most likely the BSC is a result of graphene uniformity as it overgrows steps without interruption. The BSC should be also present in other 2-d materials of current interest and can indicate optimal conditions for their growth.

Acknowledgments.

This work was supported by the U.S. Department of Energy (DOE), Office of Science, Basic Energy Sciences, Materials Science and Engineering Division. The research was performed at Ames Laboratory, which is operated for the U.S. DOE by Iowa State University under contract # DE-AC02-07CH11358. TS was supported by a Fulbright Fellowship. MHvH acknowledges funding by the Deutschemm Forschungsgemeinschaft through DFG—Project No. 278162697—SFB1242 "Nonequilibrium dynamics of condensed matter in the time domain" project B06.

References

(1) Novoselov, K. S.; Geim, A. K.; Morozov, S. V; Jiang, D.; Zhang, Y.; Dubonos, S. V; Grigorieva, I. V; Firsov, A. A. Electric Field Effect in Atomically Thin Carbon Films. *Science* **2004**, *306* (5696), 666–669.

(2) Berger, C.; Song, Z.; Li, T.; Li, X.; Ogbazghi, A. Y.; Feng, R.; Dai, Z.; Alexei, N.; Conrad, M. E. H.; First, P. N.; De Heer, W. A. Ultrathin Epitaxial Graphite: 2D Electron Gas Properties and a Route toward Graphene-Based Nanoelectronics. *J. Phys. Chem. B* **2004**, *108* (52), 19912–19916.

(3) Castro Neto, A. H.; Guinea, F.; Peres, N. M. R.; Novoselov, K. S.; Geim, A. K. The Electronic Properties of Graphene. *Rev. Mod. Phys.* **2009**, *81* (1), 109–162.

(4) Emtsev, K. V; Bostwick, A.; Horn, K.; Jobst, J.; Kellogg, G. L.; Ley, L.; McChesney, J. L.; Ohta, T.; Reshanov, S. a; Röhrl, J.; Rotenberg, E.; Schmid, A. K.; Waldmann, D.; Weber, H. B.; Seyller, T. Towards Wafer-Size Graphene Layers by Atmospheric Pressure Graphitization of Silicon Carbide. *Nat. Mater.* **2009**, *8* (3), 203–207.

(5) Petrović, M.; Hagemann, U.; Horn-von Hoegen, M.; Meyer zu Heringdorf, F. J. Microanalysis of Single-Layer Hexagonal Boron Nitride Islands on Ir(111). *Appl. Surf. Sci.* **2017**, *420*, 504–510.

(6) Chen, S.; Horn Von Hoegen, M.; Thiel, P. A.; Tringides, M. C. Diffraction Paradox: An Unusually Broad Diffraction Background Marks High Quality Graphene. *Phys. Rev. B* **2019**, *100* (15), 155307.

(7) Horn-von Hoegen, M. Growth of Semiconductor Layers Studied by Spot Profile Analysing Low Energy Electron Diffraction - Part II. *Zeitschrift fur Krist.* **1999**, *214* (11), 684–721.

(8) Mårtensson, P.; Owman, F.; Johansson, L. I. Morphology, Atomic and Electronic Structure of 6H-SiC(0001) Surfaces. *Phys. Status Solidi Basic Res.* **1997**, *202* (1), 501–528.

(9) Langer, T.; Pfnür, H.; Schumacher, H. W.; Tegenkamp, C. Graphitization Process of SiC(0001) Studied by Electron Energy Loss Spectroscopy. *Appl. Phys. Lett.* **2009**, *94* (11), 112106.

(10) Riedl, C.; Starke, U.; Bernhardt, J.; Franke, M.; Heinz, K. Structural Properties of the Graphene-SiC(0001) Interface as a Key for the Preparation of Homogeneous Large-Terrace Graphene Surfaces. *Phys. Rev. B - Condens. Matter Mater. Phys.* **2007**, *76* (24), 1–8.

(11) Owman, F.; Mårtensson, P. The SiC(0001)$6\sqrt{3} \times 6\sqrt{3}$ Reconstruction Studied with STM and LEED. *Surf. Sci.* **1996**, *369* (1–3), 126–136.

(12) Yurtsever, A.; Onoda, J.; Iimori, T.; Niki, K.; Miyamachi, T.; Abe, M.; Mizuno, S.; Tanaka, S.; Komori, F.; Sugimoto, Y. Effects of Pb Intercalation on the Structural and Electronic Properties of Epitaxial Graphene on SiC. *Small* **2016**, *12* (29), 3956–3966.

(13) Hass, J.; De Heer, W. A.; Conrad, E. H. The Growth and Morphology of Epitaxial Multilayer Graphene. *J. Phys. Condens. Matter* **2008**, *20* (32).

(14) Ohta, T.; Bostwick, A.; McChesney, J. L.; Seyller, T.; Horn, K.; Rotenberg, E. Interlayer Interaction and Electronic Screening in Multilayer Graphene Investigated with Angle-Resolved Photoemission Spectroscopy. *Phys. Rev. Lett.* **2007**, *98* (20), 206802.

(15) Nevius, M. S.; Conrad, M.; Wang, F.; Celis, A.; Nair, M. N.; Taleb-Ibrahimi, A.; Tejeda, A.; Conrad, E. H. Semiconducting Graphene from Highly Ordered Substrate Interactions. *Phys. Rev. Lett.* **2015**, *115* (3), 136802.

(16) N. Nair, M.; Palacio, I.; Celis, A.; Zobelli, A.; Gloter, A.; Kubsky, S.; Turmaud, J. P.; Conrad, M.; Berger, C.; De Heer, W.; Conrad, E. H.; Taleb-Ibrahimi, A.; Tejeda, A. Band Gap Opening Induced by the Structural Periodicity in Epitaxial Graphene Buffer Layer. *Nano Lett.* **2017**, *17* (4), 2681–2689.

(17) Hupalo, M.; Liu, X.; Wang, C.; Lu, W.; Yao, Y.; Ho, K.; Tringides, M. C. Metal Nanostructure Formation on Graphene: Weak versus Strong Bonding. *Adv. Mater.* **2011**, *23* (18), 2082–2087.

(18) Hupalo, M.; Binz, S.; Tringides, M. C. Strong Metal Adatom–Substrate Interaction of Gd and Fe with Graphene. *J. Phys. Condens. Matter* **2011**, *23* (4), 045005.

(19) Liu, X.; Wang, C.-Z.; Hupalo, M.; Lin, H.-Q.; Ho, K.-M.; Tringides, M. Metals on Graphene: Interactions, Growth Morphology, and Thermal Stability. *Crystals* **2013**, *3* (1), 79–111.

(20) Hershberger, M. T.; Hupalo, M.; Thiel, P. A.; Tringides, M. C. Growth of Fcc(111) Dy Multi-Height Islands on 6H-SiC(0001) Graphene. *J. Phys. Condens. Matter* **2013**, *25* (22), 225005.

(21) Huang, L.; Wu, Y.; Hershberger, M. T.; Mou, D.; Schrunk, B.; Tringides, M. C.; Hupalo, M.; Kaminski, A. Effects of Moiré Lattice Structure on Electronic Properties of Graphene. *Phys. Rev. B* **2017**, *96* (3), 1–6.

(22) Virojanadara, C.; Syväjarvi, M.; Yakimova, R.; Johansson, L. I.; Zakharov, A. A.; Balasubramanian, T. Homogeneous Large-Area Graphene Layer Growth on 6H-SiC(0001). *Phys. Rev. B* **2008**, *78* (24), 245403.

(23) Gulde, M.; Schweda, S.; Storeck, G.; Maiti, M.; Yu, H. K.; Wodtke, A. M.; Schafer, S.; Ropers, C. Ultrafast Low-Energy Electron Diffraction in Transmission

Resolves Polymer/Graphene Superstructure Dynamics. *Science (80-.).* **2014**, *345* (6193), 200–204.

(24) M. Hupalo, X. Liu, C. Wang, W. Lu, Y. Yao, K. Ho, and M. C. Tringides, *Adv. Mater.* 23, 2082 (2011)

(25) McDougall, D.; Hattab, H.; Hershberger, M. T.; Hupalo, M.; Horn von Hoegen, M.; Thiel, P. A.; Tringides, M. C. Dy Uniform Film Morphologies on Graphene Studied with SPA-LEED and STM. *Carbon N. Y.* **2016**, *108*, 283–290.

(26) Langer, T.; Pfnür, H.; Tegenkamp, C.; Forti, S.; Emtsev, K.; Starke, U. Manipulation of Plasmon Electron–Hole Coupling in Quasi-Free-Standing Epitaxial Graphene Layers. *New J. Phys.* **2012**, *14* (10), 103045.

(27) Supplementary materials showing characterization of samples with BSC with other techniques (STM, ARPES), its extensive presence in numerous literature experiments and in experiments for graphene grown on metals. These results further confirm the importance of BSC in identifying the growth of high quality graphene.

(28) Locatelli, A.; Knox, K. R.; Cvetko, D.; Menteş, T. O.; Niño, M. A.; Wang, S.; Yilmaz, M. B.; Kim, P.; Osgood, R. M.; Morgante, A. Corrugation in Exfoliated Graphene: An Electron Microscopy and Diffraction Study. *ACS Nano* **2010**, *4* (8), 4879–4889.

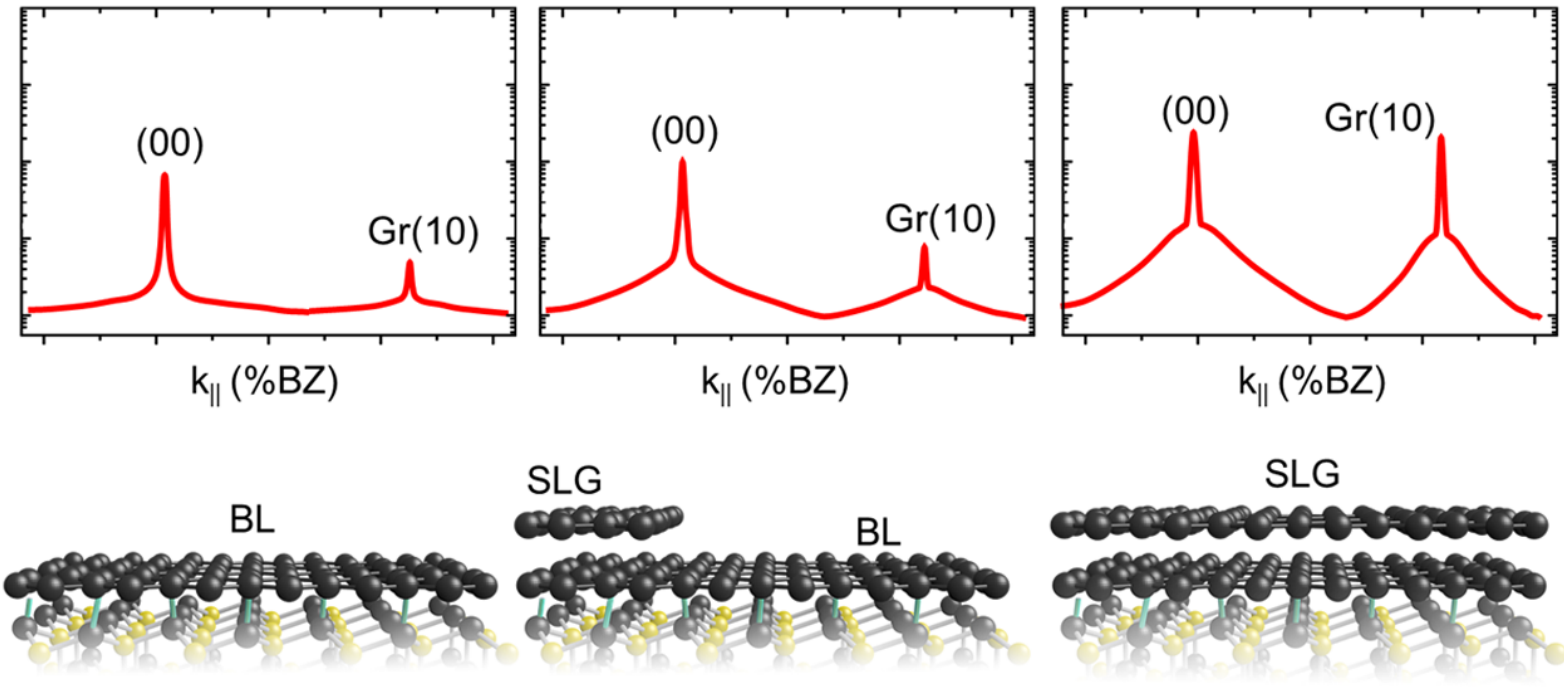
Intensity (a.u.)
(00)
Gr(10)
$k_{||}$ (%BZ)
(00)
Gr(10)
$k_{||}$ (%BZ)
(00)
Gr(10)
$k_{||}$ (%BZ)
BL
SLG
BL
SLG